Nucleic Acids Research, 2025, **53**, gkaf467
https://doi.org/10.1093/nar/gkaf467
Molecular and Structural Biology

Improved DNA binding to a type IV minor pilin increases natural transformation

Taylor J. Ellison and Courtney K. Ellison *

Department of Microbiology, University of Georgia, Athens, GA 30602, United States
*To whom correspondence should be addressed. Email: c.ellison@uga.edu

Abstract

Bacteria take up environmental DNA using dynamic appendages called type IV pili (T4P) to elicit horizontal gene transfer in a process called natural transformation. Natural transformation is widespread amongst bacteria yet the parameters that enhance or limit this process across species are poorly understood. We show that the most naturally transformable species known, *Acinetobacter baylyi*, owes this property to uniquely high levels of DNA binding by its orphan minor pilin, FimT. Expression of *A. baylyi* FimT in a closely related *Acinetobacter* pathogen substantially improves its capacity for natural transformation, showing that the acquisition of a single gene is sufficient to increase rates of horizontal gene transfer. We show that, compared with its homologs, *A. baylyi* FimT contains multiple regions of positively charged residues that additively promote DNA binding efficiency. These results demonstrate the importance of T4P–DNA binding in establishing natural transformation rates and provide a basis for improving or limiting this mechanism of horizontal gene transfer in different species.

Graphical abstract

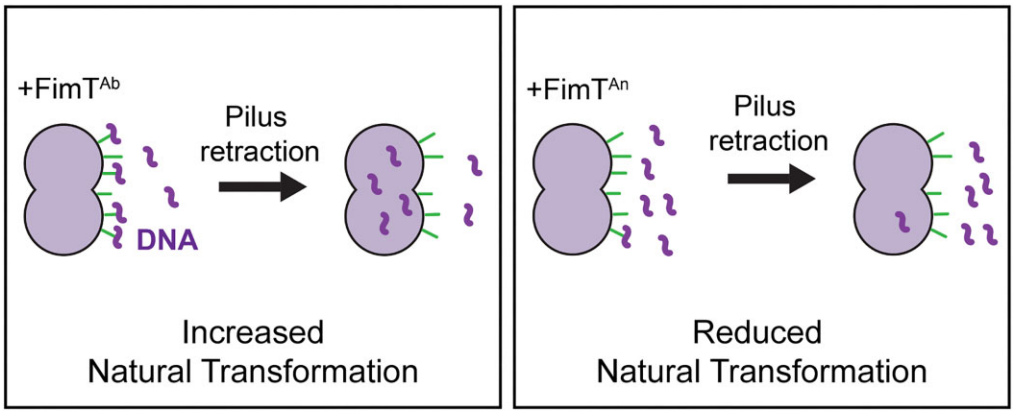

Introduction

Natural transformation has been demonstrated in upwards of 80 species [1], aiding in the spread of antibiotic resistance genes and mobile genetic elements across groups of unrelated microorganisms [2]. There are three major steps required for natural transformation: (i) DNA uptake mediated by type IV pili (T4P); (ii) DNA translocation into the cytoplasm; and (iii) incorporation of exogenous DNA into the chromosome. T4P are broadly distributed nanomachines [3] that are composed primarily of major pilin subunits that are polymerized or depolymerized via the activity of ATP-hydrolyzing motors to extend or retract [4, 5]. The exact role of T4P in DNA uptake was clarified recently when it was directly shown that pili from diverse species including T4P from *Vibrio cholerae* [6, 7] and the Gram-positive competence pili found in *Streptococcus pneumoniae* [8] and *Bacillus subtilis* [9] bind DNA to mediate DNA uptake. *Acinetobacter baylyi* is the most naturally transformable (also referred to as naturally competent) species reported in the literature, reaching transformation frequencies of up to one in two cells when grown in standard lab media such as lysogeny broth (LB) [10, 11]. *Acinetobacter baylyi* produces T4P constitutively [11], and this is one likely explanation for its high rates of natural transformation. However, species such as the pathogen *Acinetobacter nosocomialis* that can be induced for increased T4P synthesis upon surface-associated growth, only reach natural transformation frequencies of ~1 per 10 000 cells [12, 13]. Given that T4P–DNA binding is essential to the first step of DNA uptake, we hypothesized that it may be a major limiting step during natural transformation. Thus, in this study, we aimed to test

Received: October 2, 2024. **Revised:** April 24, 2025. **Editorial Decision:** April 30, 2025. **Accepted:** May 20, 2025

whether *A. baylyi* T4P have an unusually high DNA binding ability that determines transformation frequency.

Previous studies showed that minor pilins mediate DNA binding in other competent species including *V. cholerae* [6], *Neisseria* spp. [14], and *Legionella pneumophila* [15], and we suspected that a minor pilin may likewise be involved in DNA binding in *A. baylyi*. Many minor pilins are essential to T4P synthesis, with the primary model in the field suggesting that they form a complex that first primes the T4P assembly machinery to aid in the recruitment of the major pilin subunit to T4P machines [16, 17]. This prediction suggests that minor pilins assemble in a T4P tip-associated complex that is essential for T4P synthesis (Supplementary Fig. S1). *Acinetobacter baylyi* encodes six minor pilins in a conserved minor pilin operon, as well as an orphan minor pilin, FimT, located elsewhere in the chromosome (Fig. 1A). We therefore focused our transformation efficiency study by interrogating the role of minor pilins in DNA binding in *A. baylyi*. Our results show that unusually high DNA binding by its minor pilin FimT is responsible for the intrinsically elevated transformability of *A. baylyi*.

Materials and methods

Bacterial strains and culture conditions

Acinetobacter baylyi strain ADP1 was used throughout this study together with *A. nosocomialis* strain M2. For a list of strains used throughout, see Supplementary Table S1. The *A. baylyi* cultures were grown at 30°C in LB medium (unless otherwise indicated) and on agar supplemented with kanamycin (50 μg/ml), spectinomycin (60 μg/ml), gentamicin (30 μg/ml), chloramphenicol (30 μg/ml), zeocin (100 μg/ml), and/or apramycin (50 μg/ml) as appropriate. The *A. nosocomialis* cultures were grown at 37°C in LB medium and on agar supplemented with kanamycin (50 μg/ml), gentamicin (30 μg/ml), tetracycline (10 μg/ml), and/or apramycin (50 μg/ml) as appropriate.

Strain construction

Construction of mutant strains in *A. baylyi*

Mutants in *A. baylyi* were made using natural transformation as described previously [11, 18]. Briefly, mutant constructs were made by splicing-by-overlap (SOE) PCR to stitch (i) ∼3 kb of the homologous region upstream of the gene of interest; (ii) the mutation where appropriate [e.g. deletion by allelic replacement with an antibiotic [AbR] cassette]; and (iii) ∼3 kb of the homologous downstream region. For a list of primers used to generate mutants in this study, see Supplementary Table S2. The upstream region was amplified using F1 + R1 primers, and the downstream region was amplified using F2 + R2 primers. All AbR cassettes were amplified with ABD123 (ATTCCGGGGATCCGTCGAC) and ABD124 (TGTAGGCTGGAGCTGCTTC). Fusion proteins were amplified using the primers indicated in Supplementary Table S2. In-frame deletions were constructed using F1 + R1 primer pairs to amplify the upstream region and F2 + R2 primer pairs to amplify the downstream region, with ∼20 bp homology to the remaining region of the downstream region built into the R1 primer and ∼20 bp homology to the upstream region built into the F2 primer. SOE PCRs were performed using a mixture of the upstream and downstream regions, and the middle region where appropriate using F1 + R2 primers. SOE PCR products were added with 50 μl of overnight-grown culture to 450 μl of LB in 2 ml round-bottom microcentrifuge tubes (USA Scientific) and grown at 30°C rotating on a roller drum for 3–5 h. For AbR constructs, transformants were serially diluted and plated on LB and LB + antibiotic. For in-frame deletions and protein fusion constructs, after the 3–5 h incubation, cells were diluted and 100 μl of a 10^{-6} dilution was plated on LB plates. In-frame deletions were confirmed by PCR using primers ∼150 bp up- and downstream of the introduced mutation, and fusions were confirmed by sequencing. For construction of mutants containing multiple mutations that each result in transformation frequencies below the limit of detection (e.g. Δ*fimT* Δ*pilT* mutants), the parent strain was co-transformed simultaneously with PCR products containing both mutations as described above, and selected for on appropriate antibiotic plates. Each mutation introduced by co-transformations was confirmed appropriately as described above.

Complementation strains were constructed by placing the gene of interest under a constitutive P_{tac} promoter at the *vanAB* locus as described previously [11]. First, the *vanAB* locus containing the KanR and the constitutive P_{tac} promoter published previously [11] was amplified using primers 173 + 336 to amplify the upstream region. The downstream region was amplified from the same KanR-P_{tac} construct strain using primers 406 + 176. The complementation gene was then amplified using specified primers given in Supplementary Table S2. SOE PCRs and natural transformations were then performed exactly as described above. To generate *fimT* point mutations, we first constructed a P_{tac}-*fimT* strain at the *vanAB* locus as described above. We then used primers amplifying the up- and downstream regions including the P_{tac}-*fimT* region with point mutations built into the R1 and F2 primers, and carried out transformations and sequencing as described above. Because most minor pilin mutants including Δ*fimT* are not transformable, we first constructed *vanAB* expression constructs and then transformed the deletion into the expression construct strain and confirmed the deletion region by PCR and the *vanAB* locus by sequencing.

To make the P_{tac}-*fimT-3×FLAG* strain, we used genomic material from our P_{tac}-*fimT* strain as a DNA template, amplifying the upstream region including *fimT* without the stop codon with primers 173 + 2210 and the downstream region using primers 2135 + 176 where the linker for the 3×FLAG tag was built into 2210 and 2135. We then performed a second round of PCRs to introduce the 3×FLAG tag to our DNA by re-amplifying the upstream region with primers 173 + 1778 and the downstream region with primers 1777 + 176 with the 3×FLAG tags built into primers 1777 and 1778. This strain was confirmed by sequencing, and then its genomic material was used as a template to make the point mutant derivatives as described above.

Construction of mutant strains in *A. nosocomialis*

Mutants in *A. nosocomialis* were made using natural transformation and SOE products similarly to those of *A. baylyi* as described above. However, *A. nosocomialis* is not transformable in liquid media and instead requires a surface to induce competency. Strains were grown by shaking overnight in LB medium at 37°C. Then, 50 μl of overnight culture was subcultured into 3 ml of LB broth and grown with shaking for 2–3 h until cells were in the exponential growth phase. A 1 μl aliquot of exponential culture was diluted into 100 μl of

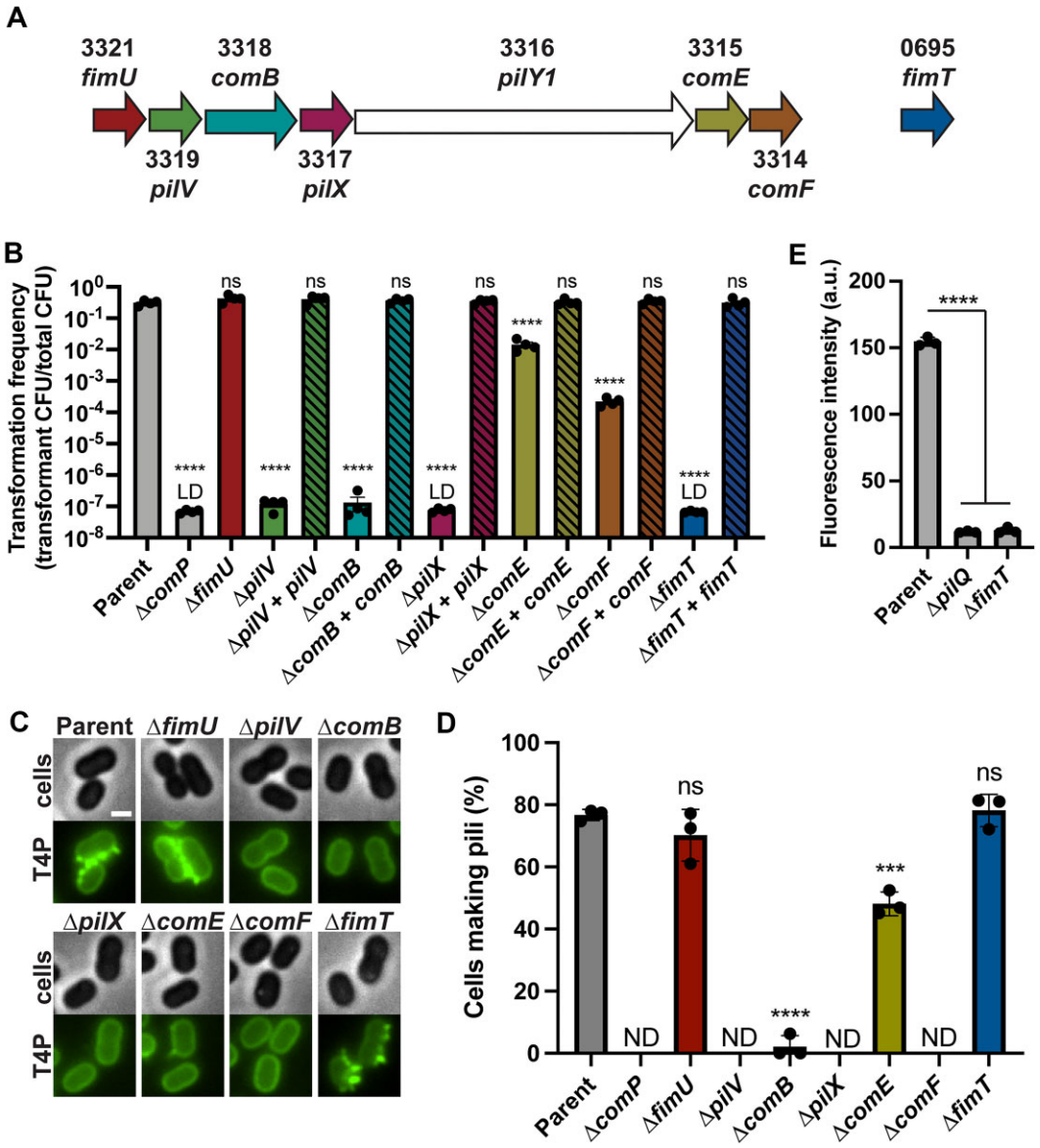

Figure 1. The minor pilin FimT is required for T4P–DNA binding but not for T4P synthesis. (**A**) Schematic of the minor pilin operon found in *A. baylyi*. Numbers indicate the ACIAD locus ID for each gene. (**B**) Natural transformation assays of the indicated strains. Each data point represents an independent, biological replicate, and bar graphs indicate the mean ± SD. The transformation frequency of the Δ*comP*, Δ*pilX*, and Δ*fimT* strains was below the limit of detection, indicated by LD. Notably, one out of four replicates from the Δ*pilV* strain and three out of four replicates from the Δ*comB* strains fell below the LD. (**C**) Representative images of the indicated strains with labeled T4P. Scale bar, 1 μm. (**D**) Quantification of the percentage of cells in populations of the indicated strains making T4P. Each data point represents an independent, biological replicate, and bar graphs indicate the mean ± SD. For each biological replicate, a minimum of 50 total cells were assessed. ND, not detected. (**E**) Quantification of Cy3-labeled DNA bound to populations of Δ*pilT* hyperpiliated strains measured using a plate reader. Each data point represents a biological replicate, and bar graphs indicate the mean ± SD. Statistics were determined by Dunnett's multiple comparisons test against the parent strain. ****$P < 0.0001$; ***$P < 0.001$; ns, not significant.

phosphate-buffered saline (PBS), and then 5–10 μl of diluted culture was mixed with ~50 ng of transforming DNA and spotted onto the surface of transformation agar (TA) (2.5 g/l NaCl, 5 g/l tryptone, 2% agarose) in microcentrifuge tubes, and incubated overnight at 30°C. The next day, cells were removed from the surface of the TA using 200 μl of PBS to resuspend surface-associated cells. Cells were then diluted and plated on LB + antibiotic plates and grown overnight at 37°C.

Because natural transformation rates in *A. nosocomialis* are significantly lower than those of *A. baylyi*, we inserted an apramycin or kanamycin resistance cassette upstream of the *pilA* locus to generate cysteine point mutations. To generate this *pilA*::*AbR*, *pilA* strain, we used primers 703 (F1) + 944 (R1) to amplify the upstream DNA and primers 943 (F2) + 744 (R2) to amplify the downstream DNA from the wild-type strain. We amplified a resistance cassette using primers ABD123 + ABD124 and then transformed the SOE product into *A. nosocomialis* and selected for the *pilA*::*AbR*, *pilA* strain on appropriate plates. The strains carrying the AbR cassettes upstream of *pilA* were confirmed by sequencing and then used as a template for generating SOE PCRs carrying

point mutations in *pilA* built into the R1 and F2 primers the same way as described above for *A. baylyi* and detailed in Supplementary Table S2. Complementation constructs in *A. nosocomialis* were also generated at the *vanAB* locus as in *A. baylyi*. P_{tac} expression constructs were first built into *A. baylyi* at the *vanAB* locus as described above and then the DNA carrying the antibiotic resistance cassette and the P_{tac} promoter was amplified using primers ABD123 + ABD124. The P_{tac} gene PCR product was then inserted into the *vanAB* locus DNA via SOE PCR, where the upstream DNA was generated using primers 1727 (F1) + 1728 (R1) and the downstream DNA was generated using primers 1729 (F2) + 688 (R2). SOE products were then transformed into *A. nosocomialis*, selected for on kanamycin, and confirmed by sequencing. To generate P_{tac}-*fimT-3×FLAG* strains, the same strategy was used as above for *A. baylyi*. Genomic material from the M2 P_{tac}-$fimT^{An}$ strain CE1202 was used as a DNA template, amplifying the upstream region including *fimT* without the stop codon with primers 1727 + 2521 and the downstream region using primers 2135 + 688 where the linker for the 3×FLAG tag was built into 2521 and 2135. A second round of PCRs introduced the 3×FLAG tag to the DNA by re-amplifying the upstream region with primers 1727 + 1778 and the downstream region with primers 1777 + 688 with the 3×xFLAG tags built into primers 1777 and 1778. This strain was confirmed by sequencing.

For construction of mutants containing multiple mutations that each result in transformation frequencies below the limit of detection (e.g. Δ*fimT* Δ*pilT* mutants), the parent strain was co-transformed simultaneously with PCR products containing both mutations as described above and selected for on appropriate antibiotic plates. Each mutation introduced by co-transformations was confirmed appropriately as described above.

To remove AbR cassettes from the indicated M2 strains, we employed a method previously described [19]. Plasmid pMMBEH*tet-flp* carrying the FLP recombinase was electroporated into strains carrying Δ*pilA*::*apr* and/or Δ*fimT*::*spec* (both apramycin and spectinomycin cassettes contain FRT sites flanking the AbR gene) and first plated on tetracycline plates to select for strains harboring the plasmid. Tet-resistant colonies were then plated on 1 mM isopropyl-β-D-thiogalactopyranoside (IPTG) plates to induce FLP recombination, and colonies on IPTG plates were subsequently grown in LB and confirmed by sequencing. FLP recombination leaves an FRT scar, indicated as ::*frt* in Supplementary Table S1.

Construction of plasmids

The plasmid pXB300 [20] that is non-replicating in *A. baylyi* was used to construct transforming plasmids utilized in DNA competition assays. First, pXB300 was amplified using primers CE1449 + CE1450, and the insert regions containing ACIAD1551::AbR were amplified from strains carrying either kanamycin or spectinomycin cassettes using primers CE1467 + CE1468. Then, amplified plasmid and insert PCR products were assembled using NEBuilder HiFi DNA Master Mix (New England Biolabs) following the manufacturer's protocols, and transformed into *Escherchia coli* strain S-17 by electroporation for maintenance and replication. *Escherichia coli* was grown in LB medium supplemented with kanamycin (50 μg/ml) or spectinomycin (60 μg/ml) where appropriate at 37°C.

Natural transformation assays

Transformation assays in *A. baylyi* were performed exactly as previously described [11, 18]. Briefly, strains were grown overnight in LB broth at 30°C on a roller drum. Then, 50 μl of overnight culture was subcultured into 450 μl of fresh LB medium, and at least 50 ng of transforming DNA (tDNA) (an ∼7 kb PCR product containing Δ*pilT*::*spec* amplified using primers CE49 + CE50) was used for all transformation assays except for DNA competition assays which are detailed below. DNA was quantified using a Qubit (ThermoFisher) following standard Qubit protocols. Reactions were incubated with end-over-end rotation on a roller drum at 30°C for 5 h and then plated for quantitative culture on LB + antibiotic plates (to quantify transformants) and on plain LB plates (to quantify total viable counts). Data are reported as the transformation frequency, which is defined as the [colony-forming units (CFU)/ml of transformants)/(CFU/ml of total viable counts].

Transformation assays in *A. nosocomialis* were performed on TA exactly as described above under mutant construction and quantified in the same way as *A. baylyi* to determine transformation frequencies. The transforming DNA used for transformations in *A. nosocomialis* was produced by PCR by amplifying an ∼7 kb region containing a gentamycin resistance cassette at locus tag FDQ49_10 705 which encodes a non-functional frameshifted gene using primers CE1788 + CE1791.

Pilin labeling, imaging, and quantification

Pilin labeling in *A. baylyi* was performed as described previously [18]. Briefly, 100 μl of overnight cultures was added to 900 μl of fresh LB in a 1.5 ml microcentrifuge tube, and cells were grown at 30°C rotating on a roller drum for 70 min. Cells were then centrifuged at 18 000 x *g* for 1 min and resuspended in 50 μl of LB before labeling with 25 μg/ml AlexaFluor488 C5-maleimide (AF488-mal) (ThermoFisher) for 15 min at room temperature. Labeled cells were centrifuged, washed three times with 100 μl of PBS, and resuspended in 5–20 μl of PBS. Cell bodies were imaged using phase-contrast microscopy while labeled pili were imaged using fluorescence microscopy on a Nikon Ti2-E microscope using a Plan Apo ×100 oil immersion objective, a GFP/FITC/Cy2 filter set for pili, a Hamamatsu ORCA-Fusion Gen-III cCMOS camera, and Nikon NIS Elements Imaging Software. Cell numbers and the percentage of cells making pili were quantified manually using Fiji. All imaging was performed under 1% agarose pads made with PBS solution.

For labeling pili in *A. nosocomialis*, cells were treated as described above with a few differences. A 50 μl aliquot of overnight cultures was diluted into 3 ml of LB and grown for 2–3 h to exponential growth phase. Then 1 ml of the liquid exponential culture was centrifuged and cells were labeled and imaged exactly as described above.

Immunofluorescence and DNA localization in Δ*fimL* Δ*pilT* mutants

We previously found that overnight cultures of *A. baylyi* grown in M63 minimal medium + casamino acids and glucose (M63CA + G) [2 g/l $(NH_4)_2SO_4$, 13.6 g/l KH_2PO_4, 0.5 mg/l $FeSO_4$, 1 mM $MgSO_4$, 0.5% w/v casamino acids, and 0.4% w/v glucose] produce longer pili than cells grown in LB [11]. We therefore grew cells in M63CA + G medium for assessing DNA and FimT localization on *A. baylyi* pili as this

increase in length vastly improved our ability to resolve individual pilus fibers. For DNA localization experiments, 100 µl of overnight cultures grown in M63CA + G were co-incubated with 25 µg/ml AF488-mal and 100 ng of fluorescently labeled DNA for 30 min. Fluorescent DNA^{Cy3} was made from an ~7 kb Δ*pilT*::*spec* PCR product that was fluorescently labeled as described previously [6] using the Cy3 LabelIT kit (Mirus Biosciences) as per the manufacturer's recommendations. Cells were washed three times with 100 µl of PBS before final resuspension in 20 µl of PBS prior to imaging. For immunofluorescence experiments, 100 µl of overnight cultures grown in M63CA + G was centrifuged and resuspended in 100 µl of PBST (PBS + 0.05% v/v Tween-20) containing a 1:100 dilution of mouse monoclonal α-FLAG antibodies (Sigma) and incubated overnight at 4°C with end-over-end rotation in a microcentrifuge tube. The next day, cells were washed three times with 200 µl of cold PBST before resuspension in 100 µl of cold PBST containing a 1:200 dilution of goat α-mouse antibodies conjugated to AlexaFluor555 (Abcam). Cells were incubated for 1 h at 4°C with end-over-end rotation before washing three times with 200 µl of cold PBST. Cells were then resuspended into 50 µl of cold PBST and incubated with 25 µg/ml AF488-mal for 15 min. Cells were then washed once with plain PBS (Tween-20 was omitted here as it has considerable background fluorescence) and then resuspended in 5–20 µl of plain PBS and imaged. A 1 µl aliquot of cells was used for microscopy employing the same microscopy setup as described above, using a DsRed/TRITC/Cy3 filter set (Nikon) to image both DNA^{Cy3} and FimT.

Western blotting

Approximately 10^9 cells from overnight cultures were concentrated into a pellet by centrifugation, and the culture supernatant was removed. Cell pellets were resuspended in 75 µl of PBS and then mixed with 25 µl of 4× SDS–PAGE sample buffer (250 mM Tris, pH 6.8, 40% glycerol, 8% SDS, 0.8% bromophenol blue, and 20% β-mercaptoethanol) and boiled using a thermal cycler set to 99°C for 10 min. Proteins were separated on a 4–20% pre-cast polyacrylamide gel (Biorad) by SDS electrophoresis, electrophoretically transferred to a nitrocellulose membrane, and probed with a 1:5000 dilution of mouse monoclonal α-FLAG antibodies (Sigma) and a 1:12 000 dilution of mouse monoclonal α-RpoA (BioLegend) primary antibodies. Blots were washed and then probed with a 1:10 000 dilution of goat α-mouse antibody conjugated to horseradish peroxidase (Sigma). Blots were subsequently incubated with SuperSignal West Pico PLUS Chemiluminescence substrate (ThermoFisher) and then imaged using a BioRad Chemidoc imaging system.

Fluorescent DNA binding assays

Hyperpiliated mutants lacking the retraction motor (Δ*pilT*) were used for all DNA binding assays to increase the dynamic range for measuring DNA binding. A 100 µl aliquot of overnight-grown cultures was added to 3 ml of fresh LB in a 14 ml culture tube (Corning) and cells were grown at 30°C rotating on a roller drum for 2–3 h. Cells were then centrifuged at 18 000 x *g* for 1 min and resuspended in 50 µl of PBS, and 100 ng of DNA^{Cy3} was added and the mixture was incubated at room temperature for 30 min. To visualize DNA binding in *pilT* mutants, cells were grown as described above, but 100 ng of DNA^{Cy3} was added to cells along with AF488-mal and incubated for 15–25 min before washing. Cells were centrifuged at 18 000 x *g* for 1 min and washed three times with 200 µl of PBS and resuspended in 200 µl of PBS. A 1 µl aliquot of cells was used for microscopy employing the same microscopy setup as described above, with a DsRed/TRITC/Cy3 filter set (Nikon) to image DNA^{Cy3}; the remaining sample was used to acquire fluorescence readings on a Synergy H1 multimode plate reader (BioTek) utilizing Gen 6 software. For DNA type binding competition assays, 100 ng of DNA^{Cy3} was added to the parent strain along with 100 ng of unlabeled ~7 kb PCR product, plasmid, or genomic (gDNA; a 1:1 ratio) and incubated for 30 min. Samples were then washed in the same way as above and subsequently measured for fluorescence intensity on the Synergy H1 multimode plate reader. Plate reader fluorescence measurements were normalized to OD_{600}.

AlphaFold modeling and DNA contact interface predictions

To predict FimT protein structures and tip complex structures bound to DNA, we used the AlphaFold3 Server [21]. Minor pilins possess N-terminal conserved pre-pilin processing G/XXXXE sites where cleavage by the pre-pilin peptidase PilD immediately after the glycine residue results in a mature pilin that can be incorporated into the T4P. To model T4P tip complexes, we used the processed forms of all minor pilins and the predicted processed form of PilY1 which is not a minor pilin but possesses an N-terminal signal sequence. Five tip complex structures were generated from each prediction, and all five showed DNA binding at the FimT–ComB interface of the T4P tip complex from both *A. baylyi* and *A. nosocomialis*. However, the models showed differences in the location of binding on the 30 bp strand of double-stranded DNA (dsDNA), with some models showing DNA binding closer to either end of the DNA strand. Because FimT can bind non-specific DNA, we expect all models to show a degree of accuracy for DNA binding, and so we chose the model with the dsDNA bound at its center for simplicity of comparison between the two species. AlphaFold modeling of tip complexes resulted in very high confidence ipTM and pTM scores (ipTM = 0.84, pTM = 0.78 for *A. baylyi*; and ipTM = 0.85, pTM = 0.78 for *A. nosocomialis*). All visualization, figure generation, and analysis of structures was performed using ChimeraX [22] software version 1.7. FimT residues within the range of charge–charge interactions with dsDNA were identified using the "Select Contacts" tool with selection parameters set to an atomic distance ≤ 10.0 Å. FimT residues within the predicted DNA–FimT interface were identified using the "Select Contacts" tool with the selection parameter for buried solvent-accessible surface area set to ≥ 0.0 $Å^2$.

Analysis of FimT DNA-binding regions

To compare DNA binding regions across FimT proteins, we first used ClustalW Multiple Sequence Alignment [23] to align 196 previously published FimT homologs [15]. Aligned regions of interest were submitted to the WebLogo 3 [24] server to generate logos for each DNA-binding region of interest, with colors distinguishing amino acid chemistry.

Statistics

All statistics were performed using GraphPad Prism software version 10.2.1.

Results

The minor pilin FimT is required for T4P–DNA binding but not T4P synthesis

To determine if specific minor pilins contribute to DNA binding, we created in-frame deletion mutants and assessed their ability to undergo natural transformation in comparison with a major pilin mutant (Δ*comP*) that does not produce T4P [11]. All minor pilin mutant strains exhibited varying degrees of defects in transformability that could be fully complemented by ectopic expression, with the exception of Δ*fimU* which has wild-type natural transformation frequencies (Fig. 1B). The high variability in transformation frequencies across different deletion strains indicates that different minor pilins may have divergent functions (Fig. 1B). Because some minor pilins are essential for T4P synthesis, we next assessed T4P phenotypes in individual minor pilin mutants. To visualize T4P, we used a previously established T4P imaging method that relies on the substitution of a cysteine residue in the major pilin subunit ComP that can then be labeled by click chemistry via fluorescent maleimide dyes [25, 26] (Fig. 1C). Microscopy experiments showed that all minor pilin mutants except for Δ*fimU* and Δ*fimT* exhibit a defect in T4P synthesis, and we conclude that the deficit in natural transformation in *pilV*, *comB*, *pilX*, *comE*, and *comF* mutants can be explained by their reduction in T4P. Notably, from these data, we cannot exclude the possibility that these minor pilins may also contribute to DNA binding (Fig. 1C, D). *fimU* mutants exhibited no defect in either natural transformation or T4P production, suggesting that FimU is involved in a different T4P function. *fimT* mutants exhibited no detectable transformation, but at the same time no defect in T4P synthesis, indicating that FimT may play a critical role in DNA binding without impacting assembly. Fluorescence-based plate reader assays that directly detect DNA binding revealed that FimT mutants show a defect in DNA binding similar to that of a mutant lacking the outer membrane secretin that is essential for T4P synthesis [18] (Δ*pilQ*), demonstrating that FimT is responsible for T4P–DNA binding (Fig. 1E).

FimT from *A. baylyi* increases transformability of the pathogen *A. noscomialis*

The pronounced phenotype whereby FimT is essential for natural transformation without impacting T4P assembly suggested that FimT may be an important factor in establishing the high natural transformation frequencies exhibited by *A. baylyi*. We thus wondered whether its expression could increase natural transformation in other bacteria. Since proteins that interact co-evolve, we reasoned that FimT from *A. baylyi* ($FimT^{Ab}$) would be less likely to interact with pilins from distantly related species, making it difficult to interrogate function. We thus focused our efforts on closely related species with lower transformation frequencies to avoid issues that may arise from disruptions in protein–protein interactions in the T4P minor pilin complex. The clinical isolate *A. nosocomialis* strain M2 was originally classified as *Acinetobacter baumannii* [27] but exhibits less innate antibiotic resistance compared with more recent clinical isolates of *A. baumannii* [28]. Both pathogens undergo natural transformation [12, 27], and their FimT homologs share 89% identity and 96% similarity [29] (Supplementary Fig. S2) so *A. nosocomialis* was employed as a model system for ease of use. The predicted structures of $FimT^{Ab}$ and $FimT^{An}$ are highly conserved, suggesting that *A. nosocomialis* would be likely to tolerate $FimT^{Ab}$ incorporation into the T4P (Supplementary Fig. S3).

We first labeled T4P in *A. nosocomialis* using a functional pilin-cysteine knockin strain (Supplementary Fig. S4) to test whether FimT was important for T4P synthesis in *Acinetobacter* pathogens. Similar to *A. baylyi*, a *fimT* deletion in *A. nosocomialis* did not impact T4P production (Fig. 2A, B), but abolished natural transformation (Fig. 2C). Ectopic complementation of its native FimT ($FimT^{An}$) restored the defect in transformability to wild-type levels of ∼1 per 10 000 cells. Strikingly, expression of $FimT^{Ab}$ resulted in a 100-fold increase in transformation relative to the wild-type strain, reaching frequencies of ∼1 per 100 cells (Fig. 2C). In contrast, expression of $FimT^{An}$ in *A. baylyi* resulted in a significant reduction in transformation frequences to ∼1 in 10 000 cells, similar to *A. nosocomialis* wild-type transformation rates (Fig. 2C). Importantly, both $FimT^{Ab}$ and $FimT^{An}$ are expressed equally in both *A. baylyi* and *A. nosocomialis* (Supplementary Fig. S5), and the expression of either protein did not affect T4P synthesis in either species (Fig. 2B). Fluorescence plate reader assays failed to detect any DNA binding by either species expressing $FimT^{An}$, suggesting that $FimT^{Ab}$ expression results in increased DNA binding (Supplementary Fig. S6). In line with natural transformation data, DNA binding by *A. nosocomialis* containing $FimT^{Ab}$ fell below the limit of detection, demonstrating that $FimT^{Ab}$ expression alone is not sufficient to achieve the DNA binding levels of wild-type *A. baylyi* (Fig. 2C). Transformation mediated by either $FimT^{Ab}$ or $FimT^{An}$ in both species is dependent on incorporation into T4P, as *fimT* expression strains lacking the major pilin in either species were not transformable (Supplementary Fig. S7). These data suggest that increased DNA binding by $FimT^{Ab}$ establishes the high rates of natural transformation of *A. baylyi*.

Multiple positively charged regions in *A. baylyi* FimT additively contribute to increased DNA binding

The two-log increase in natural transformation seen in *A. nosocomialis* expressing $FimT^{Ab}$ suggests that DNA binding by $FimT^{Ab}$ may be greater than that by other DNA-binding minor pilins. Most minor pilins are predicted to localize to the tips of T4P. One simple explanation for higher transformation in strains expressing $FimT^{Ab}$ is that $FimT^{Ab}$ may localize throughout the T4P fiber to provide increased surface area for DNA–T4P interactions. Indeed, while minor pilins are generally predicted to localize to T4P tips, some studies suggest that minor pilins can incorporate throughout the T4P fiber [30, 31]. To test whether FimT localizes to the tips or throughout T4P filaments, we performed immunofluorescence microscopy experiments with a strain encoding a largely functional *fimT-3×FLAG* (Supplementary Fig. S8). Retraction motor mutants that are incapable of T4P retraction are hyperpiliated, so mutants lacking the retraction motor (Δ*pilT*) were used to increase the number of observable T4P. However, *A. baylyi* produces its T4P close together in a line along the long axis of the cell, making it difficult to resolve individual filaments from neighboring T4P [18]. To better resolve individual T4P, we also used a Δ*fimL* mutant background, which has dispersed T4P localization but wild-type rates of natural transformation and T4P production [18] (Fig. 3A, B). For all instances where distinguishable individual T4P filaments were associated with fluorescently labeled FimT, FimT was found

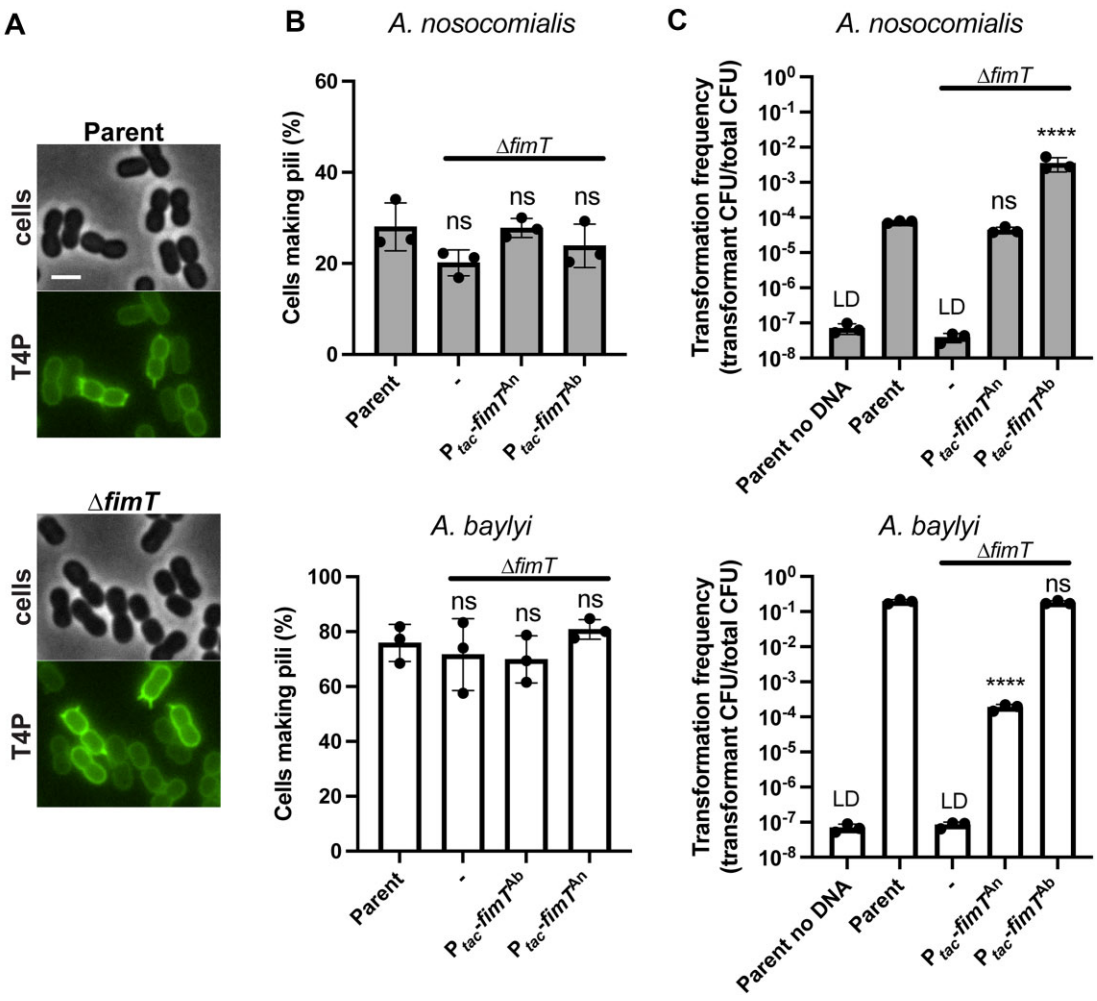

Figure 2. FimT from *A. baylyi* increases transformability of the pathogen *A. noscomialis*. (**A**) Representative images of the indicated *A. nosocomialis* strains with labeled T4P. Scale bar, 2 μm. (**B**) Quantification of the percentage of cells in populations of the indicated strains making T4P. Each data point represents a biological replicate, and bar graphs indicate the mean ± SD. For each biological replicate, a minimum of 50 total cells were assessed. (**C**) Natural transformation assays of the indicated strains. Each data point represents a biological replicate, and bar graphs indicate the mean ± SD. The transformation frequency of the no DNA control and Δ*fimT* strains was below the limit of detection, indicated by LD. Statistics were determined by Dunnett's multiple comparisons test against the parent strain. ****$P < 0.0001$; ns, not significant.

exclusively at the tips of T4P (Fig. 3A). Notably, not all T4P contain labeled FimT, which may be due to shearing of the T4P tips during wash steps associated with immunofluorescence and T4P labeling.

If FimT is the DNA-binding minor pilin, DNA should also bind the tips of T4P with FimT. To assess the localization patterns of T4P–DNA interactions, DNA was fluorescently labeled using commercially available dyes, and DNA localization was evaluated after incubation with hyperpiliated Δ*fimL* Δ*pilT* cells. As in FimT-3×FLAG immunofluorescence experiments, DNA was found almost exclusively at the tips in all instances where it co-localized with individual T4P fibers (Fig. 3B). These data are consistent with previous results from *V. cholerae* where DNA binding occurs at the tips of T4P [6], supporting a broadly applicable model where T4P bind DNA via tip-localized minor pilins and showing that differences in localization patterns do not explain increased DNA binding by FimT^{Ab}.

We next speculated that FimT may bind DNA via electrostatic charges as it does in *V. cholerae* [6]. If electrostatic interactions mediate DNA binding, then the DNA type (e.g. PCR product versus plasmid DNA or gDNA) should not influence FimT–DNA binding. To test this hypothesis, fluorescently labeled PCR products were competed against non-fluorescent genomic or plasmid DNA in a 1:1 ratio by mass. Non-fluorescent DNA, regardless of origin, reduced the fluorescent DNA signal by approximately half, as would be expected in a 1:1 fluorescent:non-fluorescent DNA mix (Supplementary Fig. S9).

Since FimT appeared to bind DNA via electrostatic charges, we applied an unbiased genetic approach to identify positions that could mediate DNA binding by individually mutating all positively charged residues within FimT to uncharged residues. Transformation frequencies of FimT mutants show the importance of the C-terminal region of FimT in natural transformation in addition to other positively charged residues (Fig. 3C). A recent study identified the C-terminus of a FimT homolog as an important region for DNA binding during natural transformation in *L. pneumophila* which reaches transformation frequencies of ∼1 in 10 000 cells [15]. Our genetic approach revealed identical residues that play a considerable role in natural transformation in *A. baylyi* and are

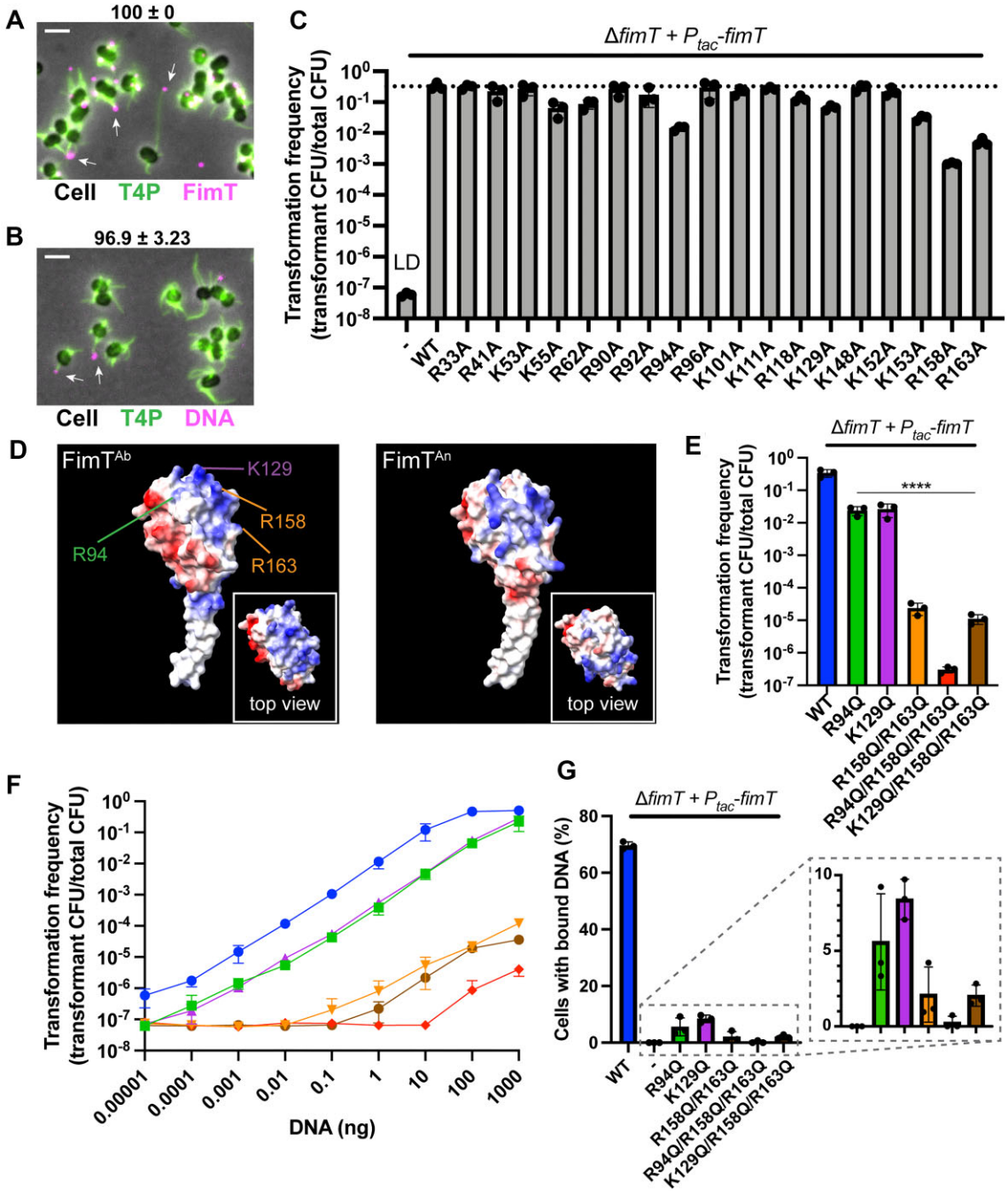

Figure 3. Multiple positively charged regions in *A. baylyi* FimT additively contribute to increased DNA binding. (A and B) Representative images of a Δ*fimL* Δ*pilT* strain with fluorescently labeled T4P (green) and immunolabeled FimT (**A**) or DNA (**B**) (fuchsia) showing FimT and DNA localization at T4P tips. Scale bars, 2 μm. Numbers above panels indicate the mean percentage of pili associated with fluorescent DNA or immunolabeled FimT-3×FLAG where the fluorescence signal was localized at the pilus tip ± SD of three biological replicates. A minimum of 30 pili associated with fluorescent puncta were quantified for each biological replicate. (**C**) Natural transformation assays of the indicated strains. A dotted line is drawn at the parent strain transformation frequency. Each data point represents an independent, biological replicate, and bar graphs indicate the mean ± SD. The transformation frequency of the uncomplemented Δ*fimT* strain was below the limit of detection, indicated by LD. (**D**) AlphaFold-predicted models of FimT from *A. baylyi* (FimT^{Ab}) and *A. nosocomialis* (FimT^{An}) showing regions of positive (blue) and negative (red) charges. (**E**) Natural transformation assays of the indicated strains containing combinatorial mutations in FimT. Each data point represents an independent, biological replicate, and bar graphs indicate the mean ± SD. Statistics were determined by Dunnett's multiple comparison test against the parent strain. ****$P < 0.0001$. (**F**) Natural transformation assays performed with increasing quantities of DNA in the indicated strains. Data show the mean ± SD of three biological replicates. (**G**) Quantification of the proportion of cells bound to Cy3-labeled DNA in the indicated strains determined by microscopy. Data points show the mean ± SD of three independent, biological replicates.

conserved in *A. noscomialis* (pre-pilin positions R158/R163 in $FimT^{Ab}$, K159/R164 in $FimT^{An}$, and R153/R158 in $FimT^{Lp}$). In addition to important C-terminal residues, $FimT^{Ab}$ possesses additional positively charged residues (K55, R62, R94, and K129) that are important for natural transformation (Fig. 3C). AlphaFold modeling predicts that R94 and K129 reside in a large region of exposed positively charged residues across the top of of $FimT^{Ab}$ that is missing from $FimT^{An}$ (Fig. 3D). We thus predicted that R94 and K129 may allow for increased DNA binding and focused on these residues to further interrogate DNA binding by $FimT^{Ab}$.

We next constructed strains containing combinatorial mutations of positively charged residues to uncharged amino acids, combining the two C-terminally encoded residues of FimT R158/R163 with either R94 or K129. Mutations to either R94 or K129 reduced transformation frequencies by 10-fold, and the R158/163 double mutant exhibited an additive decrease in transformation frequencies by 100- to 1000-fold lower than either individual mutant without affecting FimT stability (Fig. 3E; Supplementary Fig. S10). Notably, combinatorial mutations of the C-terminal positively charged residues R158/R163 did not abolish natural transformation, in contrast to *L. pneumophila* [15] where the loss of its C-terminal residues reduces transformation to below the limit of detection (Fig. 3E). The R94 mutation in combination with the R158/R163 mutations reduced transformation almost to the limit of detection, while the addition of the K129 mutation did not have a dramatic effect on natural transformation compared with the R158/R163 mutant alone. These results suggest that there may be dedicated regions of positively charged residues within FimT that additively contribute to increased DNA binding. Where K129 may act in conjunction with C-terminal residues R158/R163 to coordinate stability of DNA binding, the R94 residue may exist in an independent DNA-binding pocket, contributing to the overall increased DNA binding by FimT from *A. baylyi*.

Our transformation data indicate that FimT point mutants possess different capacities for binding DNA, and so we performed DNA titration transformation assays where we increased DNA concentrations to assess DNA binding by mutant alleles of FimT. In agreement with our hypothesis that combinatorial mutants are defective in DNA binding, DNA titration curves show that increased levels of DNA yield increase transformation rates across strains (Fig. 3F). Increasing DNA concentration in 10-fold increments resulted in concomitant 10-fold increases in transformation frequencies across strains, with the strongest defect in DNA binding exhibited by the R94/R158/R163 triple mutant. We next sought to directly quantify T4P–DNA binding in each mutant, and so we applied a microscopy approach to quantify fluorescently labeled DNA bound to cells. Microscopy experiments showed trends of DNA binding (Fig. 3G) similar to transformation rates (Fig. 3E), demonstrating that reduced DNA binding capability is responsible for the reduction in transformation frequencies in FimT mutants.

To predict how different regions could additively contribute to DNA binding in $FimT^{Ab}$, we performed AlphaFold3 [21] modeling of FimT proteins with dsDNA. FimT modeled with dsDNA alone failed to predict any protein–DNA interactions, and we speculated that modeling of the entire T4P tip complex may more accurately predict DNA–T4P binding. Transformation and T4P microscopy data from minor pilin mutants (Fig. 1B–D) and mutants lacking PilY1 [11] (which is thought to be tip associated [16, 17]) suggested that the proteins important for T4P tip complex formation and function include FimT, PilV, ComB, PilX, PilY1, ComE, and ComF. Modeling of tip components from *A. baylyi* with dsDNA robustly predicts FimT–DNA binding with the positively charged residues R94, K122, R158, and R163 identified from our genetics experiments falling within 10 Å of the DNA (the range of strong charge–charge interactions [32]) (Fig. 4A). Modeling of the tip components from *A. nosocomialis* predicts a reduction in the number of residues of $FimT^{An}$ in contact with DNA compared with $FimT^{Ab}$ (29 versus 41 residues, lime green outlines Fig. 4A), supporting a mechanism where $FimT^{Ab}$ exhibits increased DNA binding, leading to higher rates of natural transformation.

We next sought to assess the abundance of the additional DNA-binding residues identified in $FimT^{Ab}$ across FimT homologs. FimT is found in diverse clades of bacteria [15]. Comparison of the additional DNA-binding regions identified in $FimT^{Ab}$ with a set of 196 previously published FimT homologs [15] showed that while C-terminal positively charged residues are highly conserved across FimT proteins, the additional regions of $FimT^{Ab}$ that contribute to increased DNA binding are uncommon (Fig. 4B). Collectively, the data support a model where increased DNA binding by $FimT^{Ab}$ is a rare property that is achieved through the additive contributions of multiple positively charged residues. Increasing DNA binding in other species is sufficient to boost their rates of natural transformation, highlighting that DNA binding capacity determines the maximum threshold for natural transformation ability.

Discussion

Many species that have not been reported to be naturally competent under laboratory settings carry competence genes, suggesting that the phylogenetic distribution of natural transformation may be significantly underestimated [1]. There are several hypotheses for the fitness advantages that DNA uptake may confer, including nutrient salvaging from environmental DNA, the acquisition of novel genes, and the maintenance of genome fidelity by homology matching with incoming DNA [33]. Although there are many fitness advantages that could be conferred through natural competency, there are also significant disadvantages, as evidenced by the many defense systems bacteria carry to destroy foreign DNA. Few FimT homologs carry the additional positively charged regions seen in $FimT^{Ab}$, and it is likely that increased DNA binding may incur a fitness cost in different environments. Indeed it has been shown that the increased DNA binding by *A. baylyi* is associated with a fitness cost when environmental DNA is highly abundant [34]. Some species can only robustly bind DNA of close relatives via specific sequences called DNA uptake sites (DUSs) as is the case for *Haemophilus* [35] and *Neisseria* spp. [14]. DUS specificity allows for DNA exchange within related populations of cells, preventing potential issues with epigenetic mismatch and allowing sister cells to transfer genetic information. However, DUS specificity can also be co-opted to kill related species in competitive niches, as is the case in the *Neisseria* genus [36]. Commensal *Neisseria* have been shown to deploy methylated DNA containing DUSs recognized by *Neisseria gonorrhoeaea*, resulting in epigenetic incompatibility and subsequent cell death. The lack of a DUS in *A. baylyi* provides it with access to more DNA variety but also makes

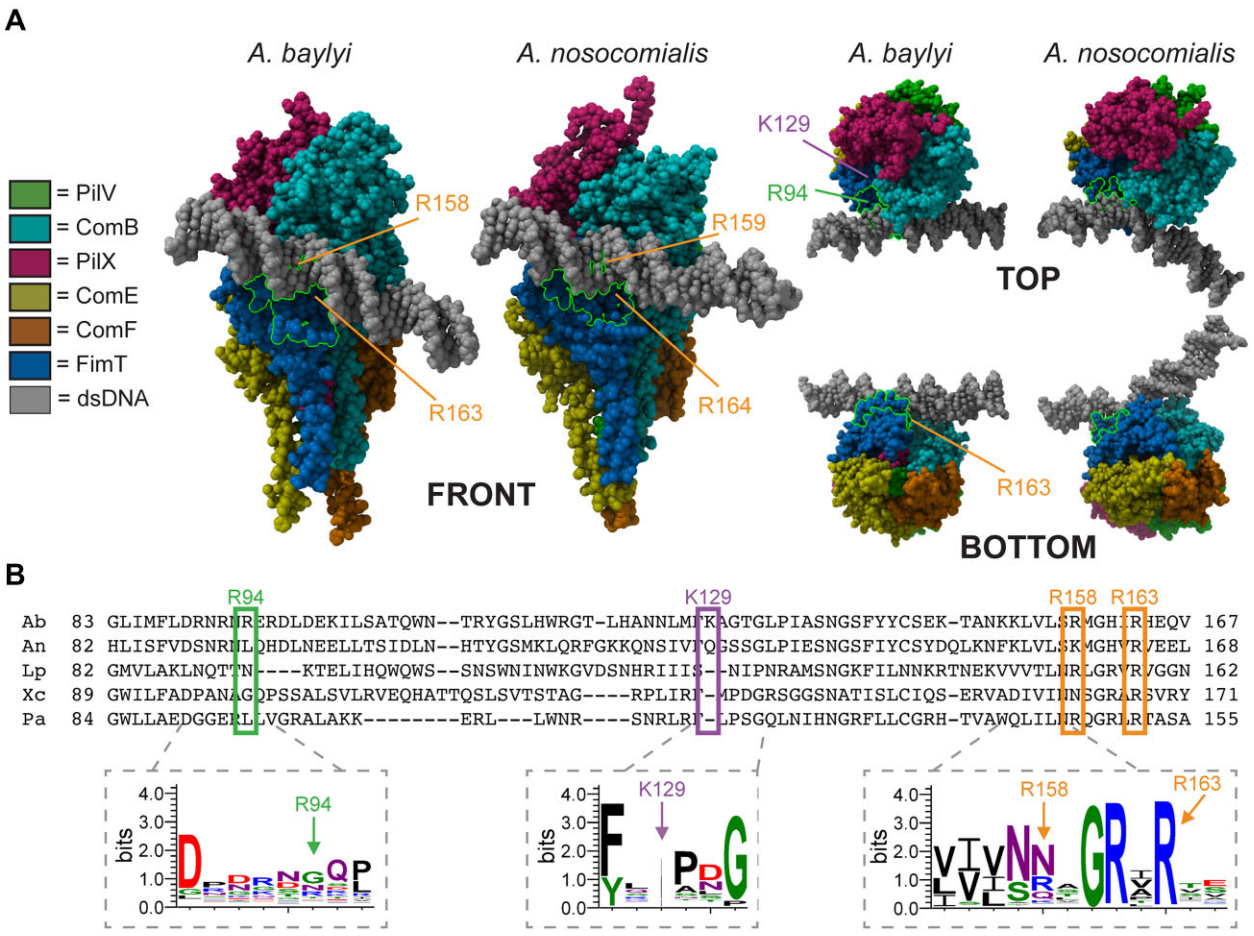

Figure 4. Additional DNA-binding regions of FimT^{Ab} are predicted to increase T4P–DNA interactions and are uncommon in other FimT homologs. (**A**) AlphaFold modeling of T4P tip complexes from *A. baylyi* or *A. nosocomialis*. Contact residues in FimT at the interface of FimT–DNA binding predicted by ChimeraX [43] are shown outlined in lime green. PilY1 is a large protein ~10-fold larger than the minor pilins (>1400 residues) and is not shown for reasons of simplicity. dsDNA 30 bp in length is shown in gray. T4P tip complex structure confidence metrics ipTM = 0.84, pTM = 0.78 for *A. baylyi* and ipTM = 0.85, pTM = 0.78 for *A. nosocomialis*. (**B**) Alignment of FimT homologs from representative species. Logos were generated from 196 previously published FimT homologs [15]. Ab, *A. baylyi*; An, *A. nosocomialis*; Lp, *Legionella pneumophila*; Xc, *Xanthomonas campestris*; Pa, *Pseudomonas aeruginosa*.

it more susceptible to epigenetic incompatibilities that could incur a fitness cost.

Interestingly, the position of the C-terminal positively charged residues of FimT^{Ab} differs slightly from those found in most FimT homologs (Fig. 4B). This suggests that DNA binding by FimT^{Ab} may require coordination of C-terminal DNA binding with DNA binding in other positively charged regions, and that repositioning of residues within DNA-binding regions could contribute to differences in binding affinity. The K129 residue is not predicted to fall in the immediate binding interface between FimT and dsDNA according to the AlphaFold3 model, in alignment with transformation data that suggest that it is involved in coordinating interactions with C-terminal residues. It is possible that the position of the K129 residue helps align the DNA for more stable interactions with C-terminal residues that are in much closer proximity to bound DNA. One interesting aspect of the AlphaFold models of the T4P tip complexes in *A. baylyi* and *A. nosocomialis* is that the minor pilin ComB may play a role in DNA binding. The models predict DNA contact with both FimT and ComB in both species; however, in *A. baylyi*, the DNA is predicted to be more enveloped by the ComB and FimT minor pilins than is seen in the model from *A. nosocomialis*. Examination of ComB within the predicted tip complex from *A. baylyi* shows that ComB has more exposed positively charged residues along the DNA-binding interface that also may contribute to increased DNA binding. It is therefore also possible that the increased DNA binding by multiple regions of FimT^{Ab} allows for more ComB–DNA interactions which may also contribute to the high rates of transformation observed in *A. baylyi*. ComB in *A. nosocomialis* does not exhibit the same positively charged interface, and this may explain why levels of transformation in *A. nosocomialis* do not fully reach *A. baylyi* frequencies when FimT^{Ab} is expressed.

Our data provide insight into additional mechanisms restricting DNA uptake and horizontal gene transfer by limiting the efficiency of T4P–DNA binding. Many bacteria limit T4P–DNA binding by reducing T4P synthesis, but this may be disadvantageous under certain conditions since T4P are often involved in multiple functions [5]. Here we present a new mechanism whereby bacteria can alter T4P–DNA binding efficiency by incorporating a unique orphan pilin. This phenomenon could be imposed as a regulatory mechanism that provides an alternative pathway for regulating T4P–DNA

binding while maintaining the production of T4P that can be used in other bacterial behaviors. We previously showed that *A. baylyi* also uses its T4P to interact with sister cells and control the spatial and structural development of three-dimensional multicellular communities [18] which has likewise been shown in the naturally competent species *V. cholerae* [7]. By employing a dedicated pilin for DNA uptake, *A. baylyi* could regulate DNA uptake capacity by limiting incorporation of FimT while still maintaining interactions with sister cells, highlighting a potential mechanism for how cells could control different T4P-related behaviors driven by the same T4P appendages. Alternatively, FimT could also contribute to other T4P functions independent of T4P production, acting as a module that regulates multiple behaviors simultaneously. Many species exhibit twitching motility in which cells use T4P retraction upon surface binding to migrate across surfaces. Although *A. baylyi* does not exhibit twitching motility under laboratory conditions [11], it is possible that this species might twitch in unidentified environmental contexts and that minor pilin switching could regulate this behavior.

There are several systems that can limit natural transformation downstream of DNA uptake. It was recently shown that some *Acinetobacter* pathogens possess restriction–modification (R-M) systems that recognize specific methylation patterns on incoming DNA to modulate transformation frequency [37]. R-M systems found in *Helicobacter pylori* and *Campylobacter jujuni* likewise prevent transformation by incoming foreign DNA [38, 39]. Intracellular nucleases targeting single-stranded DNA can also inhibit transformation rates [40], and CRISPR/Cas defense systems have been implicated in inhibiting natural transformation [41]. The cumulative results of these studies highlight the importance of regulating DNA uptake, and here we identify a new potential mechanism for controlling natural competency through DNA binding efficiency.

In many species, *fimT* genes are found in orphan loci distant from other T4P minor pilin genes that are typically encoded together in a conserved operon [15] (Fig. 1A). The genetic isolation of *fimT* indicates that it may have been horizontally acquired and that it could be transferred as a mobile T4P component via horizontal gene transfer to other species [42]. Interestingly, most other FimT homologs appear to lack the residues identified here that contribute to increased DNA binding. These results suggest that a high capacity for DNA binding may be a unique characteristic limited to few species, and exploring the fitness advantages conferred by increased DNA binding in *A. baylyi* is the subject of future study. Our finding that different regions of FimT appear to coordinate DNA binding independently suggests that increasing the number of DNA-binding sites in minor pilins from other species may permit increased DNA uptake, enabling the development of better genetic tools in genetically intractable model organisms. Ultimately, these data establish DNA binding as a major limiting step in natural transformation, providing a foundation for the development of tools that can further hinder or boost DNA binding in other species.

Acknowledgements

We are indescribably grateful for resources and laboratory space provided by M.S. Trent during early work on this project. We would also like to thank the Trent lab for the pMMBEHtet-flp plasmid; J. Engel for providing the *A. nosocomialis* M2 strain; and X. Charpentier for providing the apramycin resistance gene and helpful tips for work with *Acinetobacter* pathogens. We would also like to thank K.T. Forest, A.B. Dalia, and K.R. Hummels for critical comments on the manuscript. Courtney Ellison, PhD, is a Damon Runyon-Marilyn and Scott Urdang Breakthrough Scientist supported by the Damon Runyon Cancer Research Foundation (DFS6023).

Author contributions: C.K.E. designed and coordinated the overall study. C.K.E. and T.J.E. performed the experiments. C.K.E. and T.J.E. analyzed and interpreted the data. C.K.E. wrote the manuscript with input from T.J.E.

Supplementary data

Supplementary data are available at NAR online.

Conflict of interest

None declared.

Funding

The National Institutes of Health [R35GM150916 to C.K.E.]. The Damon Runyon Cancer Research Foundation (DFS6023).

Data availability

The data underlying this article are available in the article and in its online supplementary material.

References

1. Johnston C, Martin B, Fichant G *et al.* Bacterial transformation: distribution, shared mechanisms and divergent control. *Nat Rev Microbiol* 2014;**12**:181–96.
2. Winter M, Buckling A, Harms K *et al.* Antimicrobial resistance acquisition via natural transformation: context is everything. *Curr Opin Microbiol* 2021;**64**:133–8. https://doi.org/10.1016/j.mib.2021.09.009
3. Denise R, Abby SS, Rocha EPC. Diversification of the type IV filament superfamily into machines for adhesion, protein secretion, DNA uptake, and motility. *PLoS Biol* 2019;**17**:e3000390. https://doi.org/10.1371/journal.pbio.3000390
4. Craig L, Forest KT, Maier B. Type IV pili: dynamics, biophysics and functional consequences. *Nat Rev Microbiol* 2019;**17**:429–40.
5. Ellison CK, Whitfield GB, Brun YV. Type IV pili: dynamic bacterial nanomachines. *FEMS Microbiol Rev* 2022;**46**:429–40. https://doi.org/10.1093/femsre/fuab053
6. Ellison CK, Dalia TN, Vidal Ceballos A *et al.* Retraction of DNA-bound type IV competence pili initiates DNA uptake during natural transformation in *Vibrio cholerae*. *Nat Microbiol* 2018;**3**:773–80. https://doi.org/10.1038/s41564-018-0174-y
7. Adams DW, Stutzmann S, Stoudmann C *et al.* DNA-uptake pili of *Vibrio cholerae* are required for chitin colonization and capable of kin recognition via sequence-specific self-interaction. *Nat Microbiol* 2019;**4**:1545–57. https://doi.org/10.1038/s41564-019-0479-5
8. Lam T, Ellison CK, Eddington DT *et al.* Competence pili in *Streptococcus pneumoniae* are highly dynamic structures that retract to promote DNA uptake. *Mol Microbiol* 2021;**116**:381–96. https://doi.org/10.1111/mmi.14718
9. Zuke JD, Erickson R, Hummels KR *et al.* Visualizing dynamic competence pili and DNA capture throughout the long axis of

Bacillus subtilis. *J Bacteriol* 2023;**205**:e00156–23. https://doi.org/10.1128/jb.00156-23
10. Metzgar D, Bacher JM, Pezo V *et al.* *Acinetobacter* sp. ADP1: an ideal model organism for genetic analysis and genome engineering. *Nucleic Acids Res* 2004;**32**:5780–90. https://doi.org/10.1093/nar/gkh881
11. Ellison CK, Dalia TN, Klancher CA *et al.* *Acinetobacter baylyi* regulates type IV pilus synthesis by employing two extension motors and a motor protein inhibitor. *Nat Commun* 2021;**12**:3744. https://doi.org/10.1038/s41467-021-24124-6
12. Godeux AS, Lupo A, Haenni M *et al.* Fluorescence-based detection of natural transformation in drug-resistant *Acinetobacter baumannii*. *J Bacteriol* 2018;**200**:e00181-18. https://doi.org/10.1128/JB.00181-18
13. Vesel N, Blokesch M. Pilus production in *Acinetobacter baumannii* is growth phase dependent and essential for natural transformation. *J Bacteriol* 2021;**203**:e00034-21. https://doi.org/10.1128/JB.00034-21
14. Cehovin A, Simpson PJ, McDowell MA *et al.* Specific DNA recognition mediated by a type IV pilin. *Proc Natl Acad Sci USA* 2013;**110**:3065–70. https://doi.org/10.1073/pnas.1218832110
15. Braus SAG, Short FL, Holz S *et al.* The molecular basis of FimT-mediated DNA uptake during bacterial natural transformation. *Nat Commun* 2022;**13**:1065. https://doi.org/10.1038/s41467-022-28690-1
16. Nguyen Y, Sugiman-Marangos S, Harvey H *et al.* *Pseudomonas aeruginosa* minor pilins prime type IVa pilus assembly and promote surface display of the PilY1 adhesin. *J Biol Chem* 2015;**290**:601–11. https://doi.org/10.1074/jbc.M114.616904
17. Treuner-Lange A, Chang Y-W, Glatter T *et al.* PilY1 and minor pilins form a complex priming the type IVa pilus in *Myxococcus xanthus*. *Nat Commun* 2020;**11**:5054. https://doi.org/10.1038/s41467-020-18803-z
18. Ellison CK, Fei C, Dalia TN *et al.* Subcellular localization of type IV pili regulates bacterial multicellular development. *Nat Commun* 2022;**13**:6334. https://doi.org/10.1038/s41467-022-33564-7
19. Tucker AT, Powers MJ, Trent MS *et al.* RecET-Mediated Recombineering in Acinetobacter baumannii. In: Biswas I, Rather PN (eds.), *Acinetobacter baumannii: Methods and Protocols*. New York, NY: Springer, 2019, 107–113.
20. Bina XR, Wong EA, Bina TF *et al.* Construction of a tetracycline inducible expression vector and characterization of its use in *Vibrio cholerae*. *Plasmid* 2014;**76**:87–94. https://doi.org/10.1016/j.plasmid.2014.10.004
21. Abramson J, Adler J, Dunger J *et al.* Accurate structure prediction of biomolecular interactions with AlphaFold 3. *Nature* 2024;**630**:493–500. https://doi.org/10.1038/s41586-024-07487-w
22. Meng EC, Goddard TD, Pettersen EF *et al.* UCSF ChimeraX: Tools for structure building and analysis. *Protein Sci* 2023;**32**:e4792. https://doi.org/10.1002/pro.4792
23. Sievers F, Wilm A, Dineen D *et al.* Fast, scalable generation of high-quality protein multiple sequence alignments using Clustal Omega. *Mol Syst Biol* 2011;**7**:539. https://doi.org/10.1038/msb.2011.75
24. Crooks GE, Hon G, Chandonia J-M *et al.* WebLogo: a sequence logo generator. *Genome Res* 2004;**14**:1188–90. https://doi.org/10.1101/gr.849004
25. Ellison CK, Dalia TN, Dalia AB *et al.* Real-time microscopy and physical perturbation of bacterial pili using maleimide-conjugated molecules. *Nat Protoc* 2019;**14**:1803–19. https://doi.org/10.1038/s41596-019-0162-6
26. Ellison CK, Kan J, Dillard RS *et al.* Obstruction of pilus retraction stimulates bacterial surface sensing. *Science* 2017;**358**:535–8. https://doi.org/10.1126/science.aan5706
27. Harding CM, Tracy EN, Carruthers MD *et al.* *Acinetobacter baumannii* strain M2 produces type IV pili which play a role in natural transformation and twitching motility but not surface-associated motility. *mBio* 2013;**4**:e00360-13. https://doi.org/10.1128/mBio.00360-13
28. Sycz G, Venanzio GD, Distel JS *et al.* Modern *Acinetobacter baumannii* clinical isolates replicate inside spacious vacuoles and egress from macrophages. *PLoS Pathog* 2021;**17**:e1009802. https://doi.org/10.1371/journal.ppat.1009802
29. Stothard P. The sequence manipulation suite: javaScript programs for analyzing and formatting protein and DNA sequences. *BioTechniques* 2000;**28**:1102–4. https://doi.org/10.2144/00286ir01
30. Helaine S, Dyer DH, Nassif X *et al.* 3D structure/function analysis of PilX reveals how minor pilins can modulate the virulence properties of type IV pili. *Proc Natl Acad Sci USA* 2007;**104**:15888–93. https://doi.org/10.1073/pnas.0707581104
31. Barnier J-P, Meyer J, Kolappan S *et al.* The minor pilin PilV provides a conserved adhesion site throughout the antigenically variable meningococcal type IV pilus. *Proc Natl Acad Sci USA* 2021;**118**:e2109364118. https://doi.org/10.1073/pnas.2109364118
32. Zhou H-X, Pang X. Electrostatic interactions in protein structure, folding, binding, and condensation. *Chem Rev*. 2018;**118**:1691–741. https://doi.org/10.1021/acs.chemrev.7b00305
33. Huang M, Liu M, Huang L *et al.* The activation and limitation of the bacterial natural transformation system: the function in genome evolution and stability. *Microbiol Res* 2021;**252**:126856. https://doi.org/10.1016/j.micres.2021.126856
34. Lin L, Ringel PD, Vettiger A *et al.* DNA uptake upon T6SS-dependent prey cell lysis induces SOS response and reduces fitness of *Acinetobacter baylyi*. *Cell Rep* 2019;**29**:1633–44. https://doi.org/10.1016/j.celrep.2019.09.083
35. Mell JC, Hall IM, Redfield RJ. Defining the DNA uptake specificity of naturally competent *Haemophilus influenzae* cells. *Nucleic Acids Res* 2012;**40**:8536–49. https://doi.org/10.1093/nar/gks640
36. Kim WJ, Higashi D, Goytia M *et al.* Commensal *Neisseria* kill *Neisseria gonorrhoeae* through a DNA-dependent mechanism. *Cell Host Microbe* 2019;**26**:228–39. https://doi.org/10.1016/j.chom.2019.07.003
37. Vesel N, Iseli C, Guex N *et al.* DNA modifications impact natural transformation of *Acinetobacter baumannii*. *Nucleic Acids Res* 2023;**51**:5661–77. https://doi.org/10.1093/nar/gkad377
38. Humbert O, Dorer MS, Salama NR. Characterization of *Helicobacter pylori* factors that control transformation frequency and integration length during inter-strain DNA recombination. *Mol Microbiol* 2011;**79**:387–401. https://doi.org/10.1111/j.1365-2958.2010.07456.x
39. Beauchamp JM, Leveque RM, Dawid S *et al.* Methylation-dependent DNA discrimination in natural transformation of *Campylobacter jejuni*. *Proc Natl Acad Sci USA* 2017;**114**:E8053–61. https://doi.org/10.1073/pnas.1703331114
40. Dalia TN, Yoon SH, Galli E *et al.* Enhancing multiplex genome editing by natural transformation (MuGENT) via inactivation of ssDNA exonucleases. *Nucleic Acids Res* 2017;**45**:7527–37. https://doi.org/10.1093/nar/gkx496
41. Bikard D, Hatoum-Aslan A, Mucida D *et al.* CRISPR interference can prevent natural transformation and virulence acquisition during in vivo bacterial infection. *Cell Host Microbe* 2012;**12**:177–86.
42. Tautz D, Domazet-Lošo T. The evolutionary origin of orphan genes. *Nat Rev Genet* 2011;**12**:692–702. https://doi.org/10.1038/nrg3053
43. Meng EC, Goddard TD, Pettersen EF *et al.* UCSF ChimeraX: tools for structure building and analysis. *Protein Sci* 2023;**32**:e4792. https://doi.org/10.1002/pro.4792

Received: October 2, 2024. **Revised:** April 24, 2025. **Editorial Decision:** April 30, 2025. **Accepted:** May 20, 2025